HHS Public Access

Author manuscript

Nature. Author manuscript; available in PMC 2015 April 09.

Published in final edited form as:

Nature. 2014 October 9; 514(7521): 193–197. doi:10.1038/nature13790.

Crystal structure of a eukaryotic group II intron lariat

Aaron R. Robart[1], **Russell T. Chan**[1], **Jessica K. Peters**[1], **Kanagalaghatta R. Rajashankar**[2], and **Navtej Toor**[1,*]

[1]Department of Chemistry and Biochemistry, University of California, San Diego, La Jolla, CA

[2]NE-CAT and Department of Chemistry and Chemical Biology, Cornell University, Argonne National Laboratory, Argonne, IL 60439, USA

Abstract

The formation of branched lariat RNA is an evolutionarily conserved feature of splicing reactions for both group II and spliceosomal introns. The lariat is important for the fidelity of 5′ splice site selection and consists of a 2′-5′ phosphodiester bond between a bulged adenosine and the 5′ end of the intron. To gain insight into this ubiquitous intramolecular linkage, we determined the crystal structure of a eukaryotic group IIB intron in the lariat form at 3.7 Å. This revealed that two tandem tetraloop-receptor interactions, η-η' and π-π', place domain VI in the core to position the lariat bond in the post-catalytic state. Based on structural and biochemical data, we propose that π-π' is a dynamic interaction that mediates the transition between the two steps of splicing, with η-η' serving an ancillary role. The structure also reveals a four-magnesium-ion cluster involved in both catalysis and positioning of the 5′ end. Given the evolutionary relationship between group II and nuclear introns, it is likely that this active site configuration exists in the spliceosome as well.

Splicing of nuclear introns results in the formation of circular RNAs[1] having a branched lariat structure containing an unusual 2′-5′ phosphodiester bond[2,3]. This branched RNA product was also found in group II introns[4,5], which are self-splicing ribozymes. Defects in lariat formation result in aberrant splicing and human disease[6]. In higher eukaryotes, splicing of nuclear introns is catalyzed by a large ribonucleoprotein complex called the spliceosome, which is thought to share a common ancestor with group II introns[7,8].

Group II introns are catalytic RNAs with six structural domains (Extended Data Fig. 1) that splice via two transesterification reactions. In the first step of splicing, the 2′-OH of a bulged adenosine residue is the nucleophile that attacks the 5′ splice site to generate lariat RNA[4,5]. In the second step, the 3′-OH of the 5′ exon attacks the 3′ splice site to form ligated exons and excised intron lariat. The highly conserved domain V (DV) forms the group II intron

*Correspondence should be addressed to: N.T. (ntoor@ucsd.edu).

Author Contributions. A.R.R. and J.K.P. performed the experiments. A.R.R., R.T.C., J.K.P., and N.T. designed the experiments. A.R.R., R.T.C, J.K.P., K.R.R., and N.T. analyzed the data. A.R.R., R.T.C. and N.T. wrote the manuscript with input from all authors.

Author Information. Coordinates and structure factors have been deposited in the Protein Data Bank under accession code 4R0D. Reprints and permissions information is available at www.nature.com/reprints

The authors declare no competing financial interests

active site by binding catalytic metal ions[9], and domain VI (DVI) contains the bulged adenosine used as the nucleophile in the first step of splicing[10].

Group II introns are divided into three structural classes: IIA, IIB, and IIC[11,12]. Historically, the two model systems used to study group II intron structure and function have been "canonical" eukaryotic IIB introns: *P.li.LSUI2* from the brown algae *Pylaiella littoralis*[13] and *aI5*γ from the yeast *Saccharomyces cerevisiae*[4]. However, the only available crystal structure is of a IIC representative from the bacterium *Oceanobacillus iheyensis* (*O. iheyensis*)[9]. This idiosyncratic IIC intron class is the most primitive[14] and splices through hydrolysis to form linear intron[15]. In contrast, eukaryotic IIA and IIB introns form lariat, are evolutionarily later branching[14], and therefore more closely related to the spliceosome. We targeted the *P.li.LSUI2* intron for structure determination since it contains a functional DVI that forms large amounts of lariat during splicing[13].

Overall structure

Here we present the structure of the *P.li.LSUI2* intron in the post-catalytic lariat form with ligated exon product at 3.7 Å resolution (Extended Data Table 1a) solved using a Yb^{3+} derivative (Extended Data Fig. 2). This represents the first crystal structure of a 2′-5′ branched RNA molecule.

Reflecting the ability of IIB introns to form lariat, there are a multitude of unique tertiary interactions in the *P.li.LSUI2* intron compared to the *O. iheyensis* structure (Fig. 1). These newly visualized contacts include EBS2-IBS2 (Extended Data Fig. 3), μ-μ', ε-ε' and the canonical form of κ-κ'. Unlike the *O. iheyensis* structure, domains II and III interact with multiple domains through long-range interactions to stabilize the overall fold of the *P.li.LSUI2* intron. We can now visualize the location of DVI within the intron structure (Fig. 1; Extended Data Fig. 4), as well as the 2′-5′ lariat linkage between the first residue and the bulged adenosine.

Newly visualized tertiary interactions

One of the most highly conserved tertiary contacts in group II introns is the κ-κ' interaction between the base of the catalytic DV stem and domain I (DI)[16]. The conserved κ sequence G<u>AA</u>, nucleotide <u>A</u>171 from near the κ region, and residues from a GU<u>AA</u>C pentaloop in DIII converge to form a pentuple adenosine base stack (underlined residues) that inserts into the minor groove at the base of DV; rigidly placing the active site into the DI scaffold (Fig. 2a; Extended Data Fig. 5a).

The ε-ε' interaction is critical for catalysis, with disruption through mutagenesis resulting in complete loss of splicing activity[17]. This interaction consists of nucleotides G106 and C107 pairing with C4 and G3 from the 5′ end of the intron (Fig. 2b; Extended Data Fig. 5b). The end result of these contacts is the formation of five conserved bases stacking in the following order (from bottom to top): A573, U2, G5, C4, and G3. This serves to structure the 5′ end of the intron.

The conserved GUAA linker connecting domains I and II (J1/2) adopts an unusual backbone configuration that interacts with the 5′ end, the junction between domains II and III (J2/3), and DIII (Fig. 2c; Extended Data Fig. 5c). The 5′ end and J2/3 directly interact with the active site through J1/2 positioning these regions to stabilize the core. This new long range contact (designated as ρ-ρ') consists of two adenosines from J1/2 docking into the basal stem of DIII (Fig. 2c).

We can now correlate the function of DIII as a catalytic effector in group II introns. DIII interacts with the intron core through the aforementioned GUAAC pentaloop, which docks into the base of DV (Fig. 2d). This μ-μ' interaction[18] serves to buttress the opposite side of DV from where catalysis takes place. Furthermore, a GAAA tetraloop from DIII interacts with the base of the DII stem (designated as τ-τ') to provide additional reinforcement. Therefore, DIII functions as an external brace located on the outside surface to stabilize the entirety of the structure. This important role is consistent with deletion or mutagenesis of this domain rendering the intron unstable and not competent for efficient catalysis[19].

DII positions DVI in the active site

In the *O. iheyensis* structure, DII was drastically truncated to a small stem loop structure, and in many previous biochemical studies of the *aI5γ* intron, DII was similarly shortened to study the first step of splicing. We can now visualize the intact DII substructure and find that it serves as a central hub for four different tetraloop receptor interactions (Fig. 3a). DII makes contacts with domains I, III, and VI to organize a large portion of the intron structure.

DII has a Y-shaped RNA secondary structure with two stems D2a and D2b (Extended Data Fig. 1) coaxially stacking on top of each other such that a tetraloop receptor from D2a and a GCAA tetraloop from D2b are facing the same side (Fig. 3a). This combination provides a binding interface for DVI, which contains both a GAGA tetraloop and a tetraloop receptor. Therefore, DVI is tightly placed in the core of the intron via two tandem tetraloop receptor interactions with DII. The interaction between D2a and DVI is known as the η-η' contact[20] and we are designating the newly discovered interaction between D2b and DVI as π-π'. The π-π' interaction is especially interesting due to its proximity to the bulged adenosine residue A615, which is the nucleophile for the first step of splicing. The π tetraloop interacts with nucleotides directly adjacent to the bulged adenosine (Fig. 3a) and therefore is likely to have important effects upon the positioning of this nucleotide within the active site.

Mutagenesis of the GNRA tetraloops to UUCG was done to test the effects of these two interactions on splicing. Disrupting either contact significantly inhibited the second step of splicing, leading to an accumulation of lariat-3′ exon and 5′ exon (Fig. 3b; Extended Data Fig. 6). However, disrupting both interactions simultaneously resulted in a near complete block of the second step. This indicates that η-η' and π-π' are synergistic interactions essential for the transition to the second step of splicing and likely function through moving the 3′ splice site (which is attached to DVI) into the active site.

We can now visualize the overall fold of DVI embedded within a catalytically active intron (Fig. 3a). DVI contains a purine-rich internal loop, which forms non-canonical pairings that induce a slight bend in the helix, allowing DVI to simultaneously form both the η-η' and π-

π' contacts with DII. These interactions position the ribose sugar of the bulged A615 directly under the 5′ end of the intron. The adenosine in this 2′-5′ lariat linkage is highly constrained, since it is connected to phosphates on three different sides of the nucleotide (Extended Data Fig. 7a). The nucleobase component of the A615 residue is disordered (Fig. 3c; Extended Data Fig. 7b), which is consistent with it not playing a role in the later stages of splicing. In the current post-catalytic state, the lariat phosphodiester bond is located ~20 Å from the active site. Therefore, it has undergone a large-scale movement away from the catalytic core after the first step of splicing. In close proximity to the lariat bond, the 5′ and 3′ ends of the intron interact with each other through G1 forming a non-canonical base pair with A620 (Fig. 3c), which is important for the second step (Extended Data Fig. 6).

Active site metal ion configuration

Mg^{2+} ions are an absolute requirement for the catalysis of RNA splicing. To identify active site metal ions, soaks were performed using the anomalous scatterer Yb^{3+}, which exhibits the same octahedral coordination geometry as Mg^{2+} and preferentially binds to sites containing highly coordinated magnesium ions[9,21]. This revealed four large anomalous peaks in the ribozyme core (Fig. 4a). Two of these peaks (M1 and M2) are also found in *O. iheyensis*[9] and are embedded within DV to coordinate to the junction phosphate between the ligated exons, while the other two peaks (M3 and M4) are coordinated to the 5′ end of the intron.

M3 is located in a binding pocket formed by the highly conserved 5′ end (Extended Data Fig. 8a), which has the sequence GUGCG. Nucleotides in this region exhibit a highly contorted backbone configuration that wraps around all sides of M3 due to the ε-ε' interaction involving residues G3 and C4 (Fig. 2b). Therefore, we postulate that the primary function of ε-ε' is to order a crucial metal-binding platform which structures the 5′ end of the intron.

M4 coordinates to conserved IIB intron residues A6, C7, and A341 to further stabilize the 5′ end (Extended Data Fig. 8b). These residues are in close spatial proximity to the recently proposed ι motif (Extended Data Fig. 1) that is known to promote lariat formation and is predicted to serve as a receptor for positioning DVI[22]. An ι G79A point mutant was crystallized, revealing strong signals for M1 and M2; however, M3 and M4 were no longer visible (Extended Data Fig. 8c, d). Splicing assays of this mutant also show a negative effect on the first step of splicing (Extended Data Table 1b). Furthermore, the ε-ε' interaction, which forms the metal-binding platform for M3 and M4, persists throughout group II intron catalysis[17]. Taken together, the data suggests that M3 and M4 participate in the first step of splicing by positioning the 5′ splice site in the active site to present the scissile phosphate to M1, M2, and the bulged adenosine. However, it is possible that M3 exists only in the post-catalytic state to stabilize the repositioned lariat bond. Given the rarity of highly coordinated magnesium sites in large RNAs[23], the existence of four such metal ions in close proximity in the active site of *P.li.LSUI2* is striking. In addition, we observe a conserved monovalent ion near the M1/M2 catalytic center (Extended Data Fig. 8e).

Catalytic triplex rearrangement

In the *O. iheyensis* structure, J2/3 and residues from DV form a catalytic triplex structure essential for the catalysis of splicing and is also found in the spliceosome[24]. In the *O. iheyensis* triplex, J2/3 residues G288 and C289 (analogous to G421 and A422 in *P.li.LSUI2*) form base triples with the first two nucleotides of the catalytic triad. Unexpectedly, we observe in the *P.li.LSUI2* structure that one of the J2/3 residues is completely disengaged from the catalytic triad. Specifically, A422 has moved away from the triad and stacks directly underneath the base of the DV helix to form a base triple with residues from the J4/5 and J5/6 linkers (Fig. 4b). The possibility of J2/3 participating in conformational changes has been previously postulated[25]. However, we can now see the specific nature of this "switch" with the disengagement of J2/3 from the catalytic triad into an alternate configuration. The linkers between domains are highly conserved for each subclass of group II introns and based on the *P.li.LSUI2* structure, we hypothesize that they are dynamic and modulate splicing.

π-π' is a dynamic interaction

DVI is proposed to engage in large-scale conformational changes between the two steps of splicing[20,22]. To test this model, a catalytic triad mutant (AGC→GAU) inactive for splicing was crystallized and solved at 7 Å (Extended Data Fig. 9). Strong electron density was observed for the η-η' interaction between DII and DVI, indicating that this contact persists throughout both steps of splicing and that there is no large-scale change in DVI position. Therefore, a new model is required to explain how DVI mediates the transition between the two steps of splicing.

During the first step, the bulged adenosine must be in close proximity to M1, M2, and the 5′ splice site in order to engage in nucleophilic attack. However, π-π' places the bulged adenosine ~20 Å from the active site in the post-catalytic structure. Mutagenesis of π-π' also has no significant effect on the first step of splicing (Fig. 3b), and is unlikely to be engaged for lariat formation. Furthermore, DII is likely to remain largely stationary during catalysis due to the strong anchoring effect of multiple tetraloop receptor interactions with this domain. Based on these observations, we propose that π-π' is a dynamic interaction that toggles DVI between two different states to mediate the transition between the first and second steps of splicing (Fig. 5). In the first step, the bulged adenosine is engaged in the active site for nucleophilic attack at the 5′ splice site. At this stage, π-π' exists in the "off" state where DII is disengaged from the base of DVI. The DVI helix would also presumably exist in a relaxed conformation due to the lack of constraint provided by π-π'. Following lariat formation, DVI likely engages in remodeling of its central internal loop adjacent to A615, causing helical compression to turn "on" the π-π' interaction; thus sequestering the bulged adenosine away from the active site. A second possible model is that the base pairs between the G_6 sequence (residues 588 to 593) and a pyrimidine-rich tract (612 to 614; 616 to 618) at the proximal side of the DVI stem rearrange to reposition the lariat phosphate and engage π-π'. Both models serve to empty the active site of the 5′ end and allow entry of the 3′ splice site, which is directly attached to the end of DVI. In fact, the primary function of

the lariat may be to covalently attach to the 5′ end to provide an attachment point for this pulling action.

Evolutionary implications

This bulged adenosine of DVI is analogous to the branch site adenosine in spliceosomal introns. The branch site sequence UACUAAC (nucleophilic adenosine underlined) pairs to the U2 snRNA to extrude the adenosine from the helix[26] as in DVI. Due to the mechanistic and evolutionary similarities with group II introns, it is likely that the branch site adenosine residue and the 5′ end of nuclear introns will adopt a similar spatial arrangement relative to the catalytic core of the spliceosome. We predict that the spliceosomal branch site adenosine will be sequestered after the first step of splicing with an RNA and/or protein contact analogous to the π-π’ interaction in *P.li.LSUI2*. In fact, an interaction observed between a region just downstream of the branch site and the U5 snRNA loop may be the spliceosomal counterpart of π-π’[27].

The *P.li.LSUI2* structure provides a rationale for the phylogenetic conservation of the 5′ end. Group II introns have the consensus sequence GUGYG (Y=U or C)[11], which is similar to the GUAYG and GURAG (R=G or A) sequences found at the 5′ ends of yeast and mammalian introns, respectively[28]. In the spliceosome, the U6 snRNA pairs with the 5′ end[29] in an analogous manner to the ε-ε’ interaction in group II introns. Therefore, these conserved sequences likely form a similar metal-binding platform in spliceosomal introns, with the 5′ end forming a highly distorted backbone to coordinate magnesium ions that orient the splice site in the core.

In regards to the evolutionary rationale for the 2′-5′ phosphodiester bond, it is known that the lariat is required for full reversibility of group II intron splicing[30]. These reverse splicing reactions are the mechanism through which group II introns are able to invade DNA[31] and disperse throughout genomes. It is likely that the lariat bond pre-organizes the core of the intron structure to facilitate this reversibility. Reverse splicing has also been proposed as a vehicle for the prolific expansion of nuclear introns[32], which comprise ~25% of mammalian genomes. There is biochemical support for this hypothesis in that the spliceosome has recently been shown to catalyze reverse splicing reactions[33]. The lariat is likely to play a similar role in spliceosomal introns by allowing reverse splicing to occur, thus accounting for its phylogenetic conservation across the kingdoms by enabling “selfish introns” to replicate. Therefore, the *P.li.LSUI2* crystal structure has provided the first glimpse of the branched lariat linkage that was likely crucial for intron proliferation in eukaryotes.

Methods

Cloning and preparation of *Pylaiella littoralis LSU I2* intron RNA

DNA was synthesized (Genscript) corresponding to the second intron interrupting the large ribosomal subunit (LSU) in the mitochondria of the brown alga *Pylaiella littoralis* (*P.li.LSUI2*). The crystallization construct contains a 15-nt 5′ exon and a 5-nt 3′ exon followed by a Hind III restriction site. The DIV open reading frame (ORF) was removed from the *P.li.LSU2* intron and replaced with a UUCG stem tetraloop. This was cloned into

the EcoRV site of pUC57. Plasmid was linearized by HindIII digestion prior to *in vitro* transcription. Non-conserved loops in domain 1, 2 and 4 were changed from the wild type sequence. Most significantly, changing the sequence UAUUUAUA to UCGACAUAAGG in the ID2 stem loop improved both crystallization rate and diffraction. The final construct retained wild-type splicing activity. Transcription was performed overnight at 37°C using T7 RNA polymerase in 25 mM $MgCl_2$, 2 mM spermidine, 5 mM DTT, 40 mM Tris-HCl pH 7.5, 0.05% Triton X-100, 2.5 mM of each NTP, and thermostable inorganic pyrophosphatase (New England Biolabs). $CaCl_2$ was added to a final concentration of 1.2 mM, treated with DNase I for 45 minutes, followed by proteinase K digestion for 1 hour. The intron reacted to completion during *in vitro* transcription and was subjected to a native purification procedure previously used in the structure determination of the *O. iheyensis* intron[9]. Spliced intron RNA was repeatedly washed with 10 mM $MgCl_2$ and 5 mM sodium cacodylate pH 6.5 and concentrated to 10 mg/ml using a 100 kDa molecular weight cut-off Amicon Ultra-15 column.

Crystallization

The native crystals were grown in sitting drops by vapor diffusion at 30°C. Equal volumes of RNA (10 mg/ml) were mixed with 0.4 mM spermine, 21% 2-Methyl-2,4-pentanediol (MPD), 175 mM magnesium acetate tetrahydrate, and 90 mM MES monohydrate (pH 5.6). Rod-like crystals appeared within two days, and grew to a maximum size of 50×50×900 μm. Crystals were gradually exchanged into 21% MPD, 100 mM magnesium acetate tetrahydrate, 50 mM MES monohydrate (pH 5.6), 3 mM iridium hexammine, 0.5 mM spermine, and 100 mM NaCl; followed by flash freezing in liquid nitrogen. Iridium hexammine was used as an additive for the native crystals as it reduced mosaicity. Pre-catalytic intron RNA was obtained by mutating the AGC catalytic triad of DV to GAU. The mutation maintained stem pairing but completely inhibited splicing activity. Crystallization of this mutant was done by microseeding under conditions described above. The ι G79A mutant crystallized in 0.2 M ammonium acetate, 10 mM calcium chloride, 50 mM sodium cacodylate pH 6.5, and 10% w/v polyethylene glycol 4000. Resulting crystals were cryoprotected through gradual transfer to the crystallization solution supplemented with 30% ethylene glycol.

Structure determination

The crystal structure of the *P.li.LSUI2* intron was solved at 3.7 Å resolution using multi-wavelength anomalous dispersion (MAD) with crystals soaked in 0.5 mM ytterbium (III) chloride. Yb^{3+} soaks were performed in 21% MPD, 100 mM magnesium acetate tetrahydrate, 50 mM MES monohydrate (pH 5.6), 0.5 mM spermine, 100 mM NaCl, and 0.5 mM $YbCl_3$ for 3 hours at room temperature. Tl^+ soaks were performed in the same manner with 10 mM thallium acetate. X-ray data sets were collected at NE-CAT's 24-ID-C beamline at the Advanced Photon Source (Argonne National Laboratory, Argonne, Illinois). Data was processed using HKL-2000[34], heavy metal sites were identified with SHELXD[35] and phasing done using Phenix[36] and SHELXE[37]. RNA nucleotides were modeled using COOT[38] and the RCrane plugin[39]. The phylogenetically predicted secondary structure (Extended Data Fig. 1) guided modeling into the electron density. Structure refinement was done using Buster[40], Phenix[36], DEN[41], and Phenix.Erasser[42]. The 2′-5′ phosphodiester bond

was restrained using a cif restraint file in phenix.refine. All software was compiled by SBGrid[43].

In vitro self-splicing assays

The construct used for the *in vitro* self-splicing assays contained wild-type *P.li.LSUI2* sequence with DIV ORF removed and a 250-nt 5′ exon and 75-nt 3′ exon. This was cloned into the pUC57 plasmid. Plasmid was linearized using HindIII and used for *in vitro* transcription with T7 RNA polymerase. Radiolabeled transcripts were prepared as above using 10 μCi [α-32P] UTP (3000 Ci/mmole), 0.5 mM UTP, 1 mM other NTPs, and 10mM $MgCl_2$. Transcripts were gel purified on a 4% polyacrylamide (19:1)/8 M urea gel, RNA was recovered by diffusion into 300 mM NaCl, 0.01% SDS, 1 mM EDTA. Self-splicing experiments were performed for 30 min at 45°C in a splicing buffer containing 10 mM $MgCl_2$, 1M NH_4Cl, 40 mM Tris-HCl (pH 7.5), and 0.02% SDS. Reactions were stopped by addition of EDTA to a final concentration of 20 mM. Splicing products were resolved using a denaturing 4% polyacrylamide (19:1)/8 M urea gels. Rate constants for the WT and G79A mutant were derived from curves fit to a biphasic exponential equation. All splicing assays were done in triplicate.

Extended Data

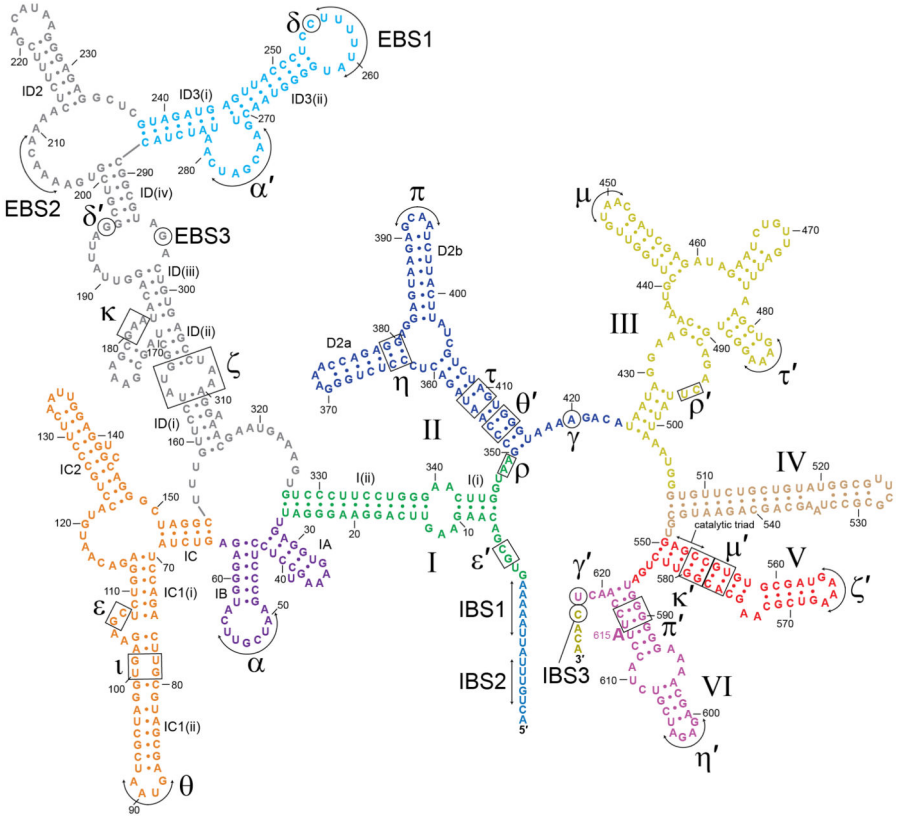

Extended Data Figure 1.

Secondary structure of *P.li.LSUI2* intron crystallization construct. Tertiary interactions are indicated with Greek letters and domains are labeled with Roman numerals. Colouring of the individual domains is consistent with the overall view of the tertiary structure shown in Fig. 1.

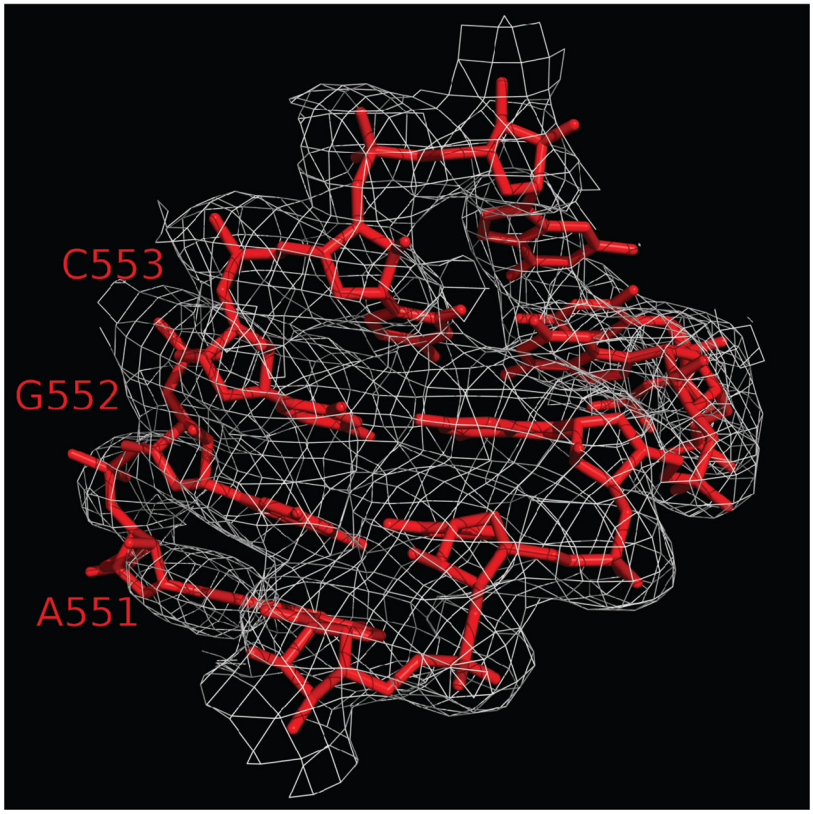

Extended Data Figure 2.
The Yb-MAD experimental, density modified map of the portion of DV containing the catalytic triad contoured at 1.8σ.

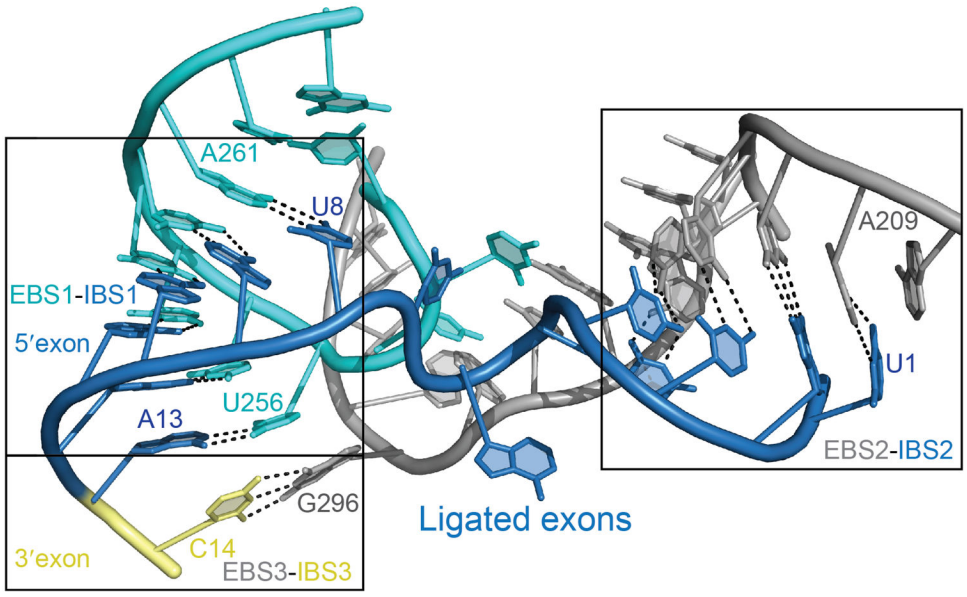

Extended Data Figure 3.

The path of the 5′ exon through the intron structure. The EBS1-IBS1 and EBS2-IBS2 interactions position the 5′ exon. They do not form a continuous binding interface with the presence of a highly distorted backbone at the junction between these two motifs. As a result, the helical axes of the EBS1-IBS1 and EBS2-IBS2 pairings are positioned ~90° relative to each other. The EBS3-IBS3 interaction places the 3′ exon in the active site.

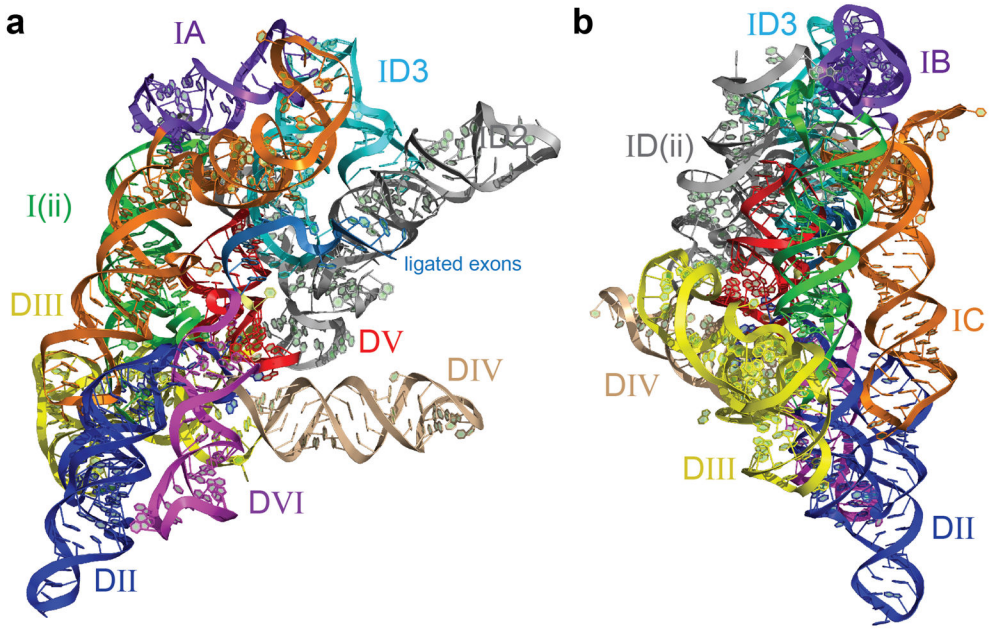

Extended Data Figure 4.

Overall tertiary structure of the *P.li.LSUI2* intron. Individual domains and subdomains are depicted in different colors. Domain names are labeled with Roman numerals. **a** and **b** show different rotations of the intron structure.

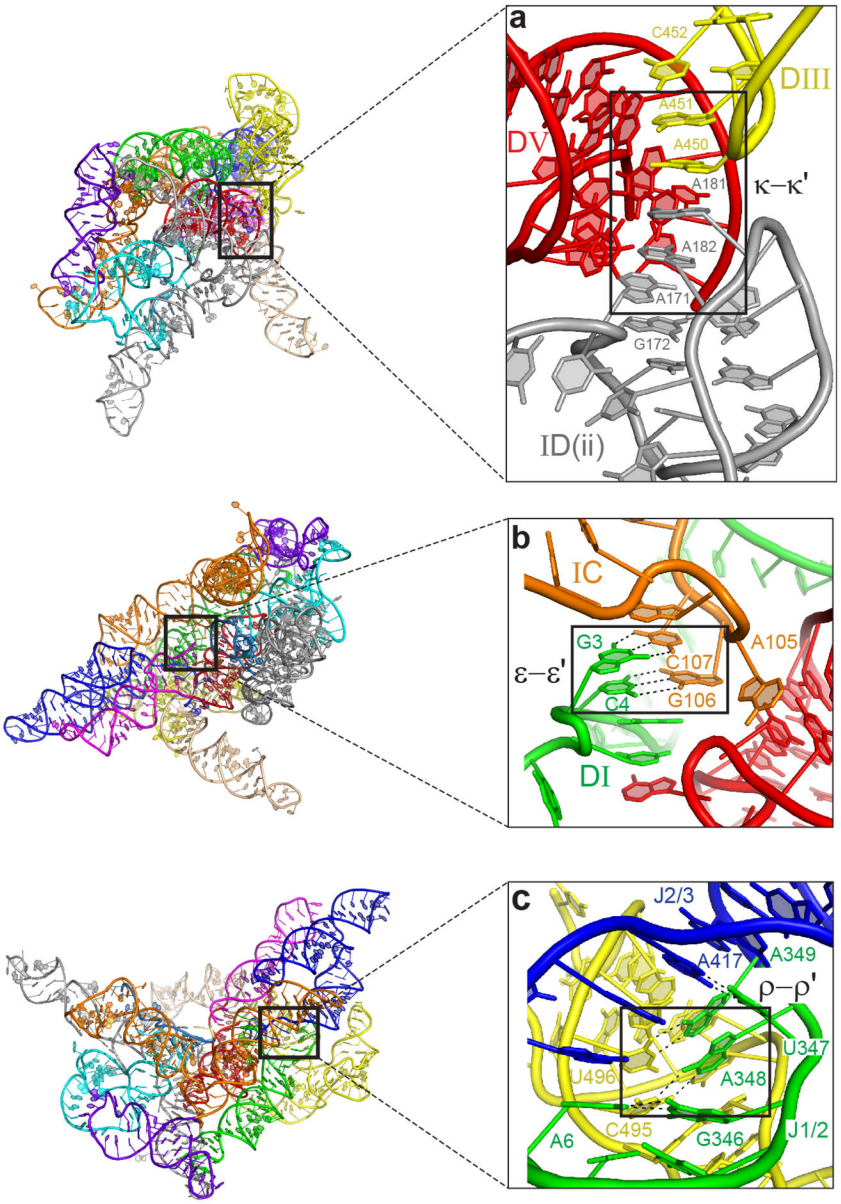

Extended Data Figure 5.

Companion to Fig. 2 showing the location of the individual tertiary interactions relative to the overall structure.

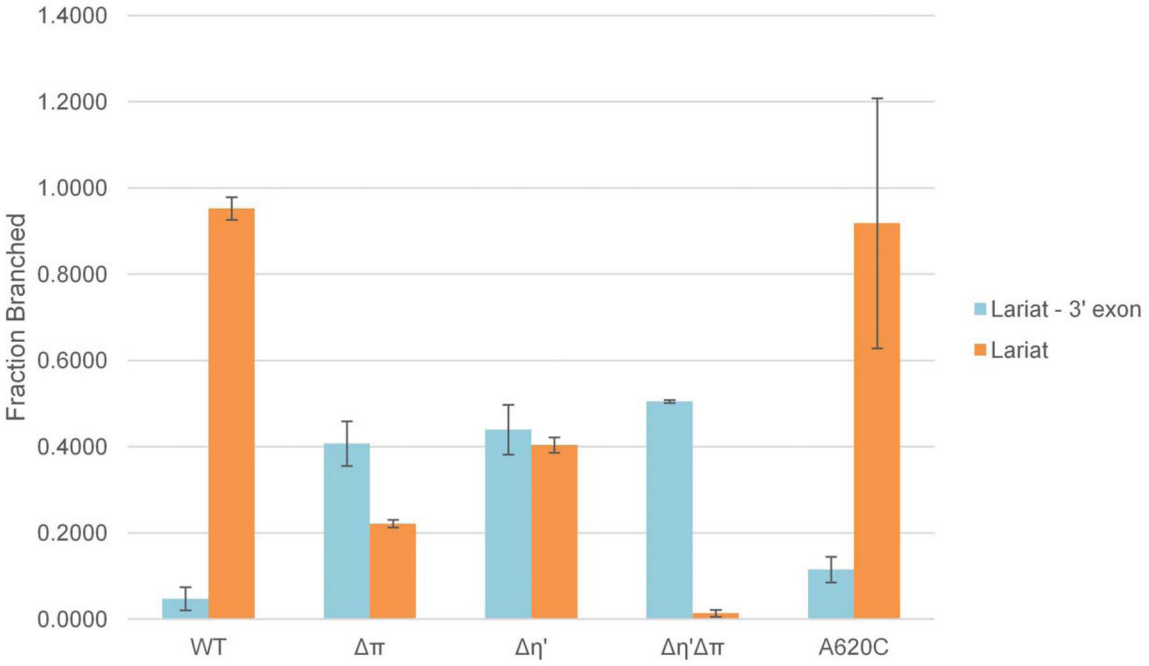

Extended Data Figure 6.

Splicing assays for the DVI mutants showing the proportion of branched product. Blue and orange bars correspond to lariat-3′ exon and lariat, respectively. The Δη' and Δπ mutants accumulate large amounts of lariat-3′ exon, thus indicating a second step splicing defect. The Δη'Δπ double mutant is almost completely blocked before the second step. The A620C mutant shows 2.4-fold greater accumulation of lariat-3′ exon compared to the WT intron indicating that the interaction between G1 and A620 is important for the second step. In the yeast *aI5γ* intron, G1 instead interacts with the penultimate residue[44], indicating a certain degree of flexibility for this pairing. There is evidence for a similar interaction between the termini of nuclear introns[45] involving nearby (but not exactly equivalent) residues, which also has a significant effect upon the second step of splicing. Therefore, the 5′ and 3′ ends of nuclear introns may have a similar arrangement within the spliceosome.

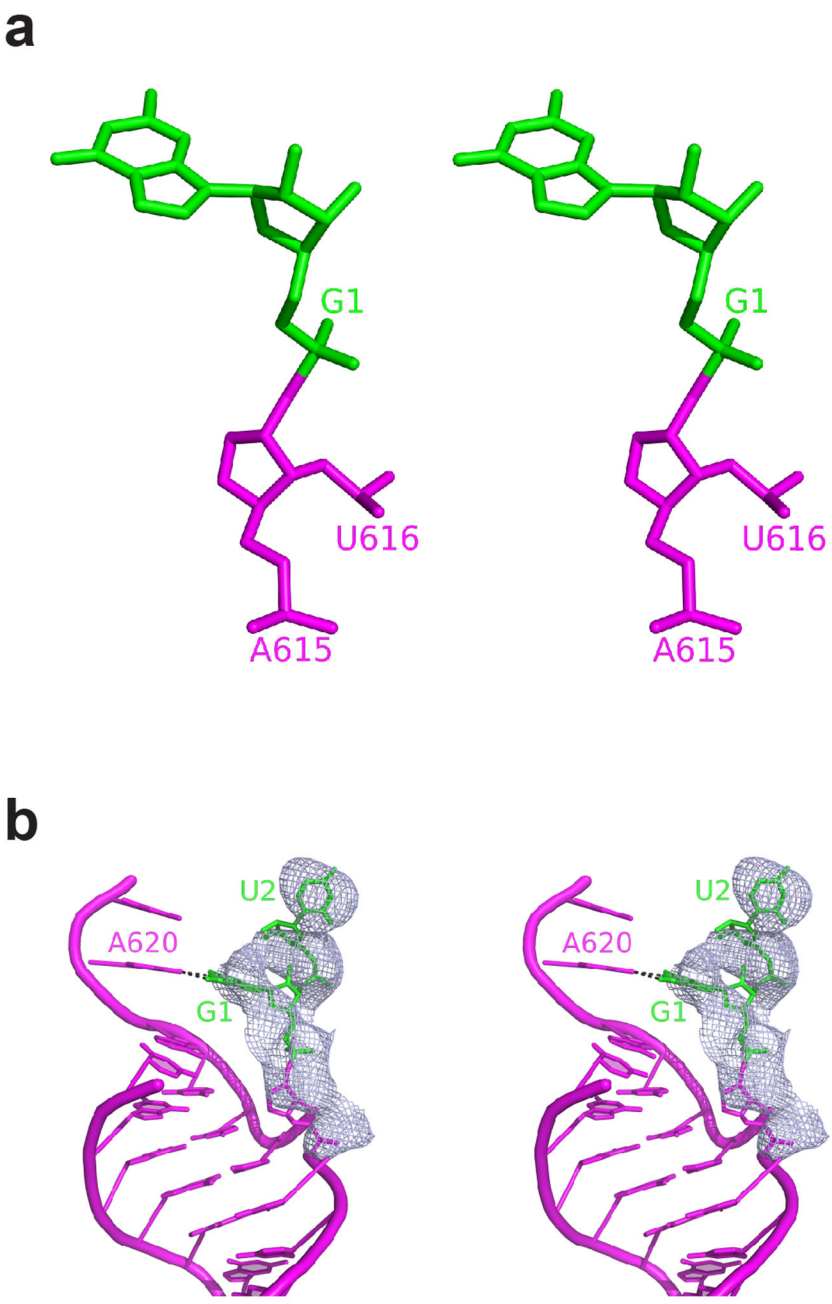

Extended Data Figure 7.

a, The lariat 2′-5′ phosphodiester bond in wall-eyed stereo format. **b**, Stereo version of Fig. 3c. See Fig. 3c legend for details. F_o-F_c density for the lariat bond contoured at 3σ.

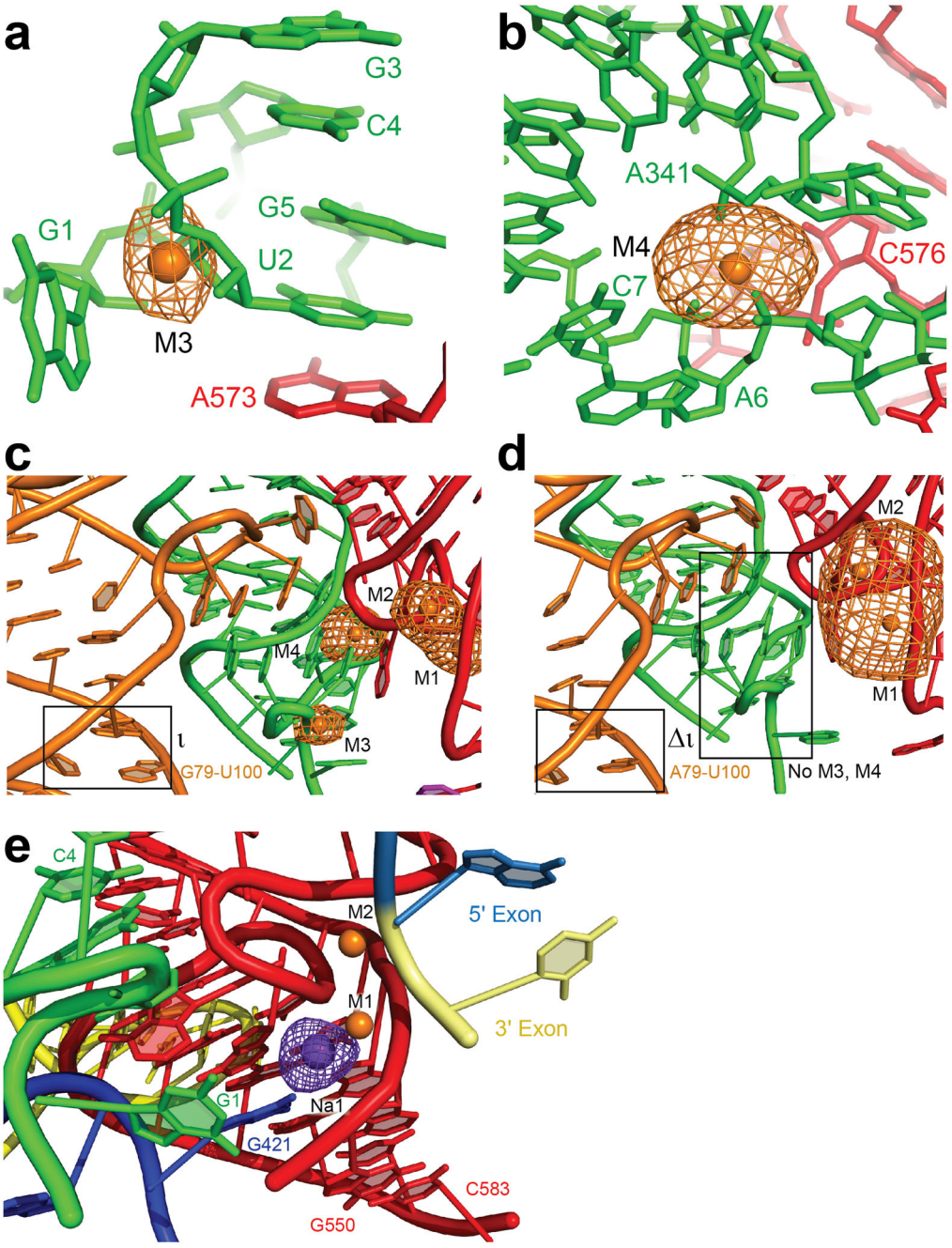

Extended Data Figure 8.

a and **b** depict the RNA ligands surrounding metals M3 and M4, respectively. Yb^{3+} anomalous map contoured at 9σ. **c**, Yb^{3+} anomalous map for WT contoured at 9σ. **d**, Compared with the WT intron, the Yb^{3+} anomalous map for the ι G79A mutant (contoured at 4σ) is lacking the peaks corresponding to M3 and M4, even at a lower contour level. **e**, Tl^{+} was used as a probe for monovalent ions in the RNA structure[46]. The Tl^{+} anomalous map (purple mesh contoured at 5.5σ) revealed a strong peak located 3.8 Å from M1 that coordinates to the nucleobase of J2/3 residue G421 and the backbone of DV nucleotide

G550. This sodium ion Na1 (purple sphere) is significantly closer to M1 than the equivalent K^+ ion found in *O. iheyensis*[25]. Otherwise, this monovalent ion binding site is relatively conserved between these two introns.

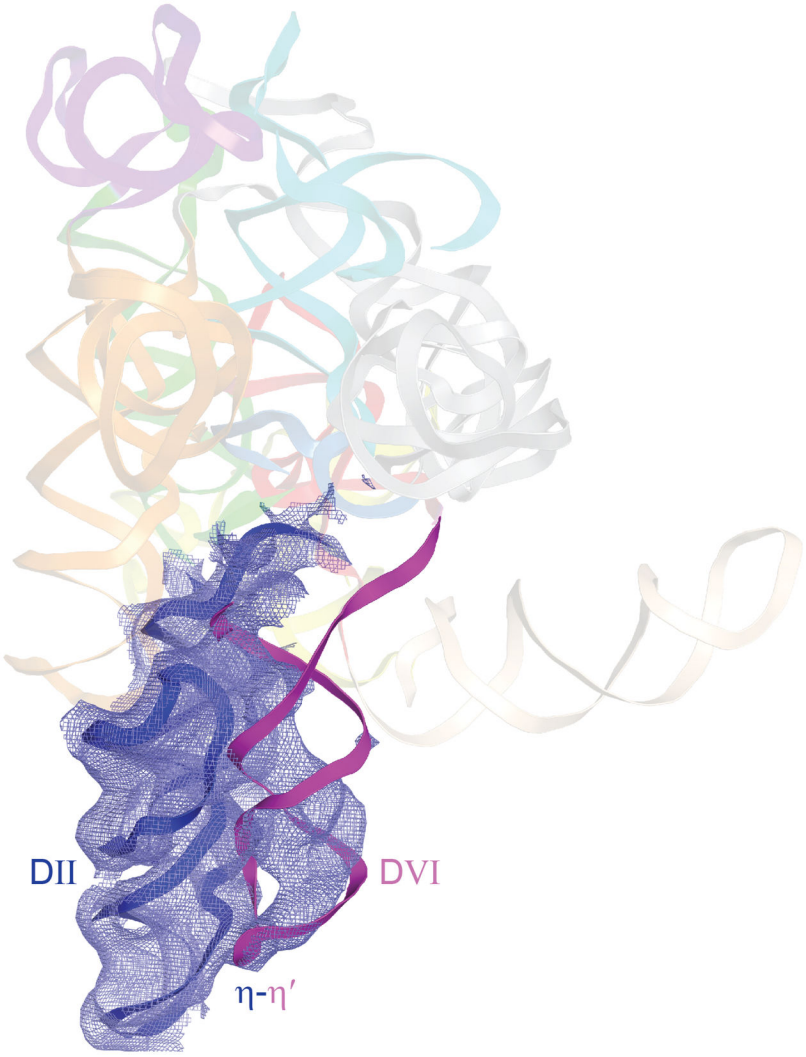

Extended Data Figure 9.

$2F_o$-F_c density for DVI in the pre-catalytic structure contoured at 1σ. The η-η' interaction persists throughout the splicing reaction and is visible in the pre-catalytic state. The weaker density for the central region of DVI suggests a partially disordered, dynamic region with possible helical remodeling in the conserved internal loop during splicing. The general pattern of side-by-side packing of domains II and VI persists between the two steps. Catalytic triad mutation consisted of an AGC→GAU substitution.

Extended Data Table 1a

	P.li.LSUI2 native	DV Triad Mutant	G79A Mutant	Yb^{3+}		
Data collection				Peak	Inflection	
Space group	$C222_1$	$C222_1$	C222	$C222_1$	$C222_1$	
Cell						
a, *b*, *c* (Å)	163.7, 255.4, 136.8	161.9, 264.5, 137.5	211.7, 457.2, 179.5	164.6, 257.7, 138.0		161.2
α, β, γ (°)	90, 90, 90	90, 90, 90	90, 90, 90	90, 90, 90	90, 90, 90	9
Wavelength (eV)	11218.5	12662	8949.5	8949.5	8946.5	
Resolution (Å)	150.0-3.68 (3.74-3.68)	50.0-7.25 (7.37-7.25)	50.0-9.75 (9.92-9.75)	50.0-4.65 (4.73-4.65)	50.0-4.49 (4.57-4.49)	50.0-4
R_{sym}	14.9 (>100)	9.5 (77.9)	8.6 (97.0)	8.8 (73.9)	9.2 (72.8)	8
$I/\sigma I$	6.4 (0.6)	13.2 (1.7)	14.3 (1.8)	16.1 (2.1)	9.2 (1.2)	2
Completeness	99.9 (99.9)	94.6 (82.5)	96.3 (96.9)	99.9 (99.6)	97.9 (88.7)	9
Redundancy	6.8 (3.8)	5.7 (4.7)	6.5 (6.0)	4.4 (3.7)	3.6 (2.8)	
CC*	(0.743)					
Refinement						
Resolution (Å)	81.8-3.68					
No. reflections	31107					
R_{work}/R_{free}	23.9/27.4					
No. atoms	13979					
RNA	13471					
Ligand/ion	393					
Water	115					
B-factors						
RNA	201.6					
Ligand/ion	181.5					
Water	177.0					
R.m.s.						
Bond lengths	0.017					
Bond angles	1.483					

*Highest resolution shell is shown in parenthesis.

Extended Data Table 1b

	k_{fast} (min^{-1})	k_{slow} (min^{-1})
WT	9.51 ± 1.09	0.136 ± 0.0246
G79A	2.97 ± 1.57	0.0767 ± 0.00942

Supplementary Material

Refer to Web version on PubMed Central for supplementary material.

Acknowledgments

We thank Surajit Banerjee and the staff of the NE-CAT beamlines at the Advanced Photon Source (APS) of Argonne National Laboratory. We thank Partho Ghosh, Simpson Joseph, Gourisankar Ghosh, Russell Doolittle, Yitzhak Tor, Dan Donoghue, and Timothy Wiryaman for comments on the manuscript. We thank Rhiju Das and Fang-Chieh Chou for assistance with phenix.erasser for structure refinement and Gerard Bricogne for advice on Buster refinement. We also thank Nicole T. Schirle for preliminary biochemical characterization of the *P.li.LSUI2* intron. R.T.C. was supported by the Cell, Molecular, and Genetics Training Program funded by NIH predoctoral training grant 5T32GM007240. J.K.P. was supported by the UCSD Molecular Biophysics Training Program funded by NIH predoctoral training grant 5T32GM008326. NE-CAT is supported by NIH grant 8P41GM103403-10 and APS is supported by the U.S. DOE under Contract No. DE-AC02-06CH11357. This work was supported by a Hellman Foundation Fellowship and NIH grant 5R01GM102216 awarded to N.T.

References

1. Grabowski PJ, Padgett RA, Sharp PA. Messenger RNA splicing in vitro: an excised intervening sequence and a potential intermediate. Cell. 1984; 37:415–427. [PubMed: 6722880]
2. Padgett RA, Konarska MM, Grabowski PJ, Hardy SF, Sharp PA. Lariat RNA's as intermediates and products in the splicing of messenger RNA precursors. Science. 1984; 225:898–903. [PubMed: 6206566]
3. Konarska MM, Grabowski PJ, Padgett RA, Sharp PA. Characterization of the branch site in lariat RNAs produced by splicing of mRNA precursors. Nature. 1985; 313:552–557. [PubMed: 2578627]
4. Peebles CL, et al. A self-splicing RNA excises an intron lariat. Cell. 1986; 44:213–223. [PubMed: 3510741]
5. van der Veen R, et al. Excised group II introns in yeast mitochondria are lariats and can be formed by self-splicing in vitro. Cell. 1986; 44:225–234. [PubMed: 2417726]
6. Di Leo E, et al. A point mutation in the lariat branch point of intron 6 of NPC1 as the cause of abnormal pre-mRNA splicing in Niemann-Pick type C disease. Hum Mutat. 2004; 24:440. [PubMed: 15459971]
7. Galej WP, Oubridge C, Newman AJ, Nagai K. Crystal structure of Prp8 reveals active site cavity of the spliceosome. Nature. 2013; 493:638–643. [PubMed: 23354046]
8. Fica SM, et al. RNA catalyses nuclear pre-mRNA splicing. Nature. 2013; 503:229–234. [PubMed: 24196718]
9. Toor N, Keating KS, Taylor SD, Pyle AM. Crystal structure of a self-spliced group II intron. Science. 2008; 320:77–82. [PubMed: 18388288]
10. Lambowitz AM, Zimmerly S. Group II introns: mobile ribozymes that invade DNA. Cold Spring Harb Perspect Biol. 2011; 3
11. Toor N, Hausner G, Zimmerly S. Coevolution of group II intron RNA structures with their intron-encoded reverse transcriptases. RNA. 2001; 7:1142–1152. [PubMed: 11497432]
12. Michel F, Umesono K, Ozeki H. Comparative and functional anatomy of group II catalytic introns--a review. Gene. 1989; 82:5–30. [PubMed: 2684776]
13. Costa M, Fontaine JM, Loiseaux-de Goër S, Michel F. A group II self-splicing intron from the brown alga *Pylaiella littoralis* is active at unusually low magnesium concentrations and forms populations of molecules with a uniform conformation. J Mol Biol. 1997; 274:353–364. [PubMed: 9405145]
14. Rest JS, Mindell DP. Retroids in archaea: phylogeny and lateral origins. Mol Biol Evol. 2003; 20:1134–1142. [PubMed: 12777534]
15. Toor N, Robart AR, Christianson J, Zimmerly S. Self-splicing of a group IIC intron: 5′ exon recognition and alternative 5′ splicing events implicate the stem-loop motif of a transcriptional terminator. Nucleic Acids Res. 2006; 34:6461–6471. [PubMed: 17130159]
16. Boudvillain M, Pyle AM. Defining functional groups, core structural features and inter-domain tertiary contacts essential for group II intron self-splicing: a NAIM analysis. EMBO J. 1998; 17:7091–7104. [PubMed: 9843513]
17. Jacquier A, Michel F. Base-pairing interactions involving the 5′ and 3′-terminal nucleotides of group II self-splicing introns. J Mol Biol. 1990; 213:437–447. [PubMed: 2191139]

18. Fedorova O, Pyle AM. A conserved element that stabilizes the group II intron active site. RNA. 2008; 14:1048–1056. [PubMed: 18441048]
19. Fedorova O, Mitros T, Pyle AM. Domains 2 and 3 interact to form critical elements of the group II intron active site. J Mol Biol. 2003; 330:197–209. [PubMed: 12823961]
20. Chanfreau G, Jacquier A. An RNA conformational change between the two chemical steps of group II self-splicing. EMBO J. 1996; 15:3466–3476. [PubMed: 8670849]
21. Adams PL, Stahley MR, Kosek AB, Wang J, Strobel SA. Crystal structure of a self-splicing group I intron with both exons. Nature. 2004; 430:45–50. [PubMed: 15175762]
22. Li CF, Costa M, Michel F. Linking the branchpoint helix to a newly found receptor allows lariat formation by a group II intron. EMBO J. 2011; 30:3040–3051. [PubMed: 21712813]
23. Klein DJ, Moore PB, Steitz TA. The contribution of metal ions to the structural stability of the large ribosomal subunit. RNA. 2004; 10:1366–1379. [PubMed: 15317974]
24. Fica SM, Mefford MA, Piccirilli JA, Staley JP. Evidence for a group II intron-like catalytic triplex in the spliceosome. Nat Struct Mol Biol. 2014; 21:464–471. [PubMed: 24747940]
25. Marcia M, Pyle AM. Visualizing group II intron catalysis through the stages of splicing. Cell. 2012; 151:497–507. [PubMed: 23101623]
26. Query CC, Moore MJ, Sharp PA. Branch nucleophile selection in pre-mRNA splicing: evidence for the bulged duplex model. Genes Dev. 1994; 8:587–597. [PubMed: 7926752]
27. Anokhina M, et al. RNA structure analysis of human spliceosomes reveals a compact 3D arrangement of snRNAs at the catalytic core. EMBO J. 2013; 32:2804–2818. [PubMed: 24002212]
28. Parker R, Guthrie C. A point mutation in the conserved hexanucleotide at a yeast 5′ splice junction uncouples recognition, cleavage, and ligation. Cell. 1985; 41:107–118. [PubMed: 2986840]
29. Lesser CF, Guthrie C. Mutations in U6 snRNA that alter splice site specificity: implications for the active site. Science. 1993; 262:1982–1988. [PubMed: 8266093]
30. Roitzsch M, Pyle AM. The linear form of a group II intron catalyzes efficient autocatalytic reverse splicing, establishing a potential for mobility. RNA. 2009; 15:473–482. [PubMed: 19168748]
31. Yang J, Zimmerly S, Perlman PS, Lambowitz AM. Efficient integration of an intron RNA into double-stranded DNA by reverse splicing. Nature. 1996; 381:332–335. [PubMed: 8692273]
32. Lynch M, Richardson AO. The evolution of spliceosomal introns. Curr Opin Genet Dev. 2002; 12:701–710. [PubMed: 12433585]
33. Tseng CK, Cheng SC. Both catalytic steps of nuclear pre-mRNA splicing are reversible. Science. 2008; 320:1782–1784. [PubMed: 18583613]
34. Otwinowski Z, Minor W. Processing of X-ray diffraction data collected in oscillation mode. Methods in Enzymology. 1997; 276:307–326.
35. Schneider TR, Sheldrick GM. Substructure solution with SHELXD. Acta Crystallogr D Biol Crystallogr. 2002; 58:1772–1779. [PubMed: 12351820]
36. Adams PD, et al. PHENIX: a comprehensive Python-based system for macromolecular structure solution. Acta Crystallogr D Biol Crystallogr. 2010; 66:213–221. [PubMed: 20124702]
37. Sheldrick GM. A short history of SHELX. Acta Crystallogr A. 2008; 64:112–122. [PubMed: 18156677]
38. Emsley P, Cowtan K. Coot: model-building tools for molecular graphics. Acta Crystallogr D Biol Crystallogr. 2004; 60:2126–2132. [PubMed: 15572765]
39. Keating KS, Pyle AM. RCrane: semi-automated RNA model building. Acta Crystallogr D Biol Crystallogr. 2012; 68:985–995. [PubMed: 22868764]
40. Blanc E, et al. Refinement of severely incomplete structures with maximum likelihood in BUSTER-TNT. Acta Crystallogr D Biol Crystallogr. 2004; 60:2210–2221. [PubMed: 15572774]
41. Schroder GF, Levitt M, Brunger AT. Super-resolution biomolecular crystallography with low-resolution data. Nature. 2010; 464:1218–1222. [PubMed: 20376006]
42. Chou FC, Sripakdeevong P, Dibrov SM, Hermann T, Das R. Correcting pervasive errors in RNA crystallography through enumerative structure prediction. Nat Methods. 2013; 10:74–76. [PubMed: 23202432]

43. Morin A, et al. Collaboration gets the most out of software. Elife. 2013; 2:e01456. [PubMed: 24040512]

44. Chanfreau G, Jacquier A. Interaction of intronic boundaries is required for the second splicing step efficiency of a group II intron. EMBO J. 1993; 12:5173–5180. [PubMed: 8262060]

45. Parker R, Siliciano PG. Evidence for an essential non-Watson-Crick interaction between the first and last nucleotides of a nuclear pre-mRNA intron. Nature. 1993; 361:660–662. [PubMed: 8437627]

46. Basu S, et al. A specific monovalent metal ion integral to the AA platform of the RNA tetraloop receptor. Nat Struct Biol. 1998; 5:986–992. [PubMed: 9808044]

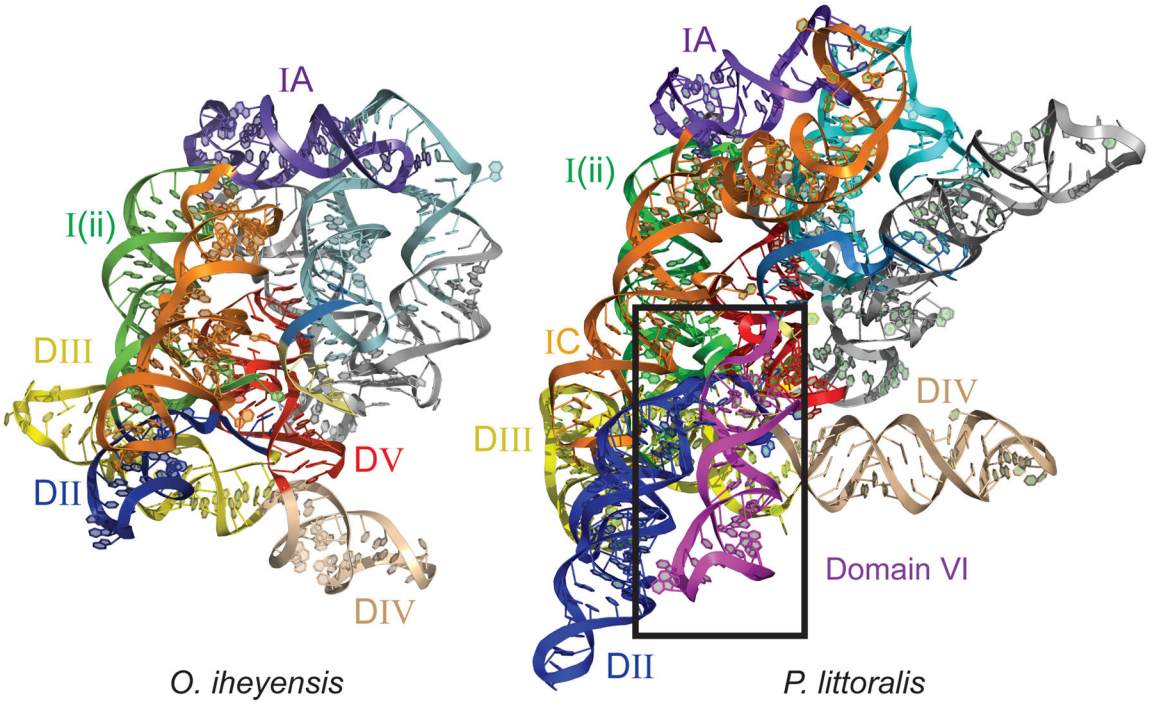

Figure 1.

A comparison of the tertiary structures of *O. iheyensis* and *P.li.LSUI2* group II introns. *P.li.LSUI2* has a significantly larger and more complex structure with a correspondingly greater number of unique RNA tertiary contacts. Domain VI of *P.li.LSUI2* is highlighted within the box.

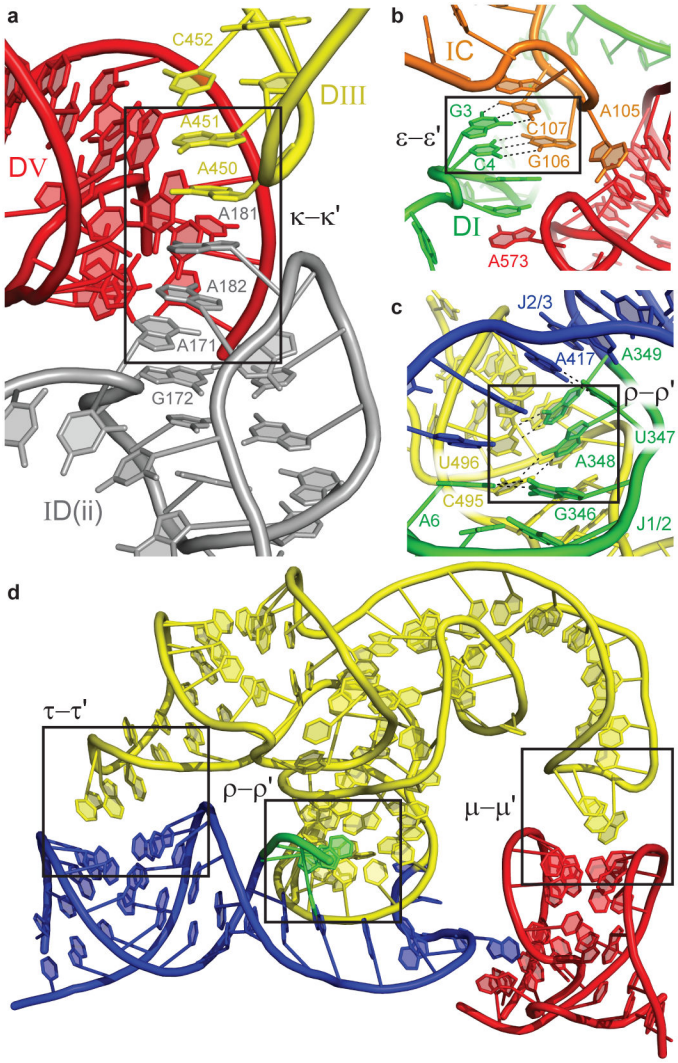

Figure 2.

Tertiary interactions in a IIB intron. **a**, The κ loop (grey) and DIII (yellow) converge to form an extended base stack involving five adenosine residues inserting into the minor groove of DV (red). **b**, G106 and C107 form Watson-Crick pairs with C4 and G3 from the 5′ end to form the ε-ε' interaction that positions the 5′ end in the active site. **c**, J1/2 (green) interacts with the 5′ end (A6 residue in green), DIII (yellow), and J2/3 (blue). **d**, DIII (yellow) acts as a brace on the surface of the intron and forms three tertiary interactions (boxed) with DI (green), DII (blue) and DV (red).

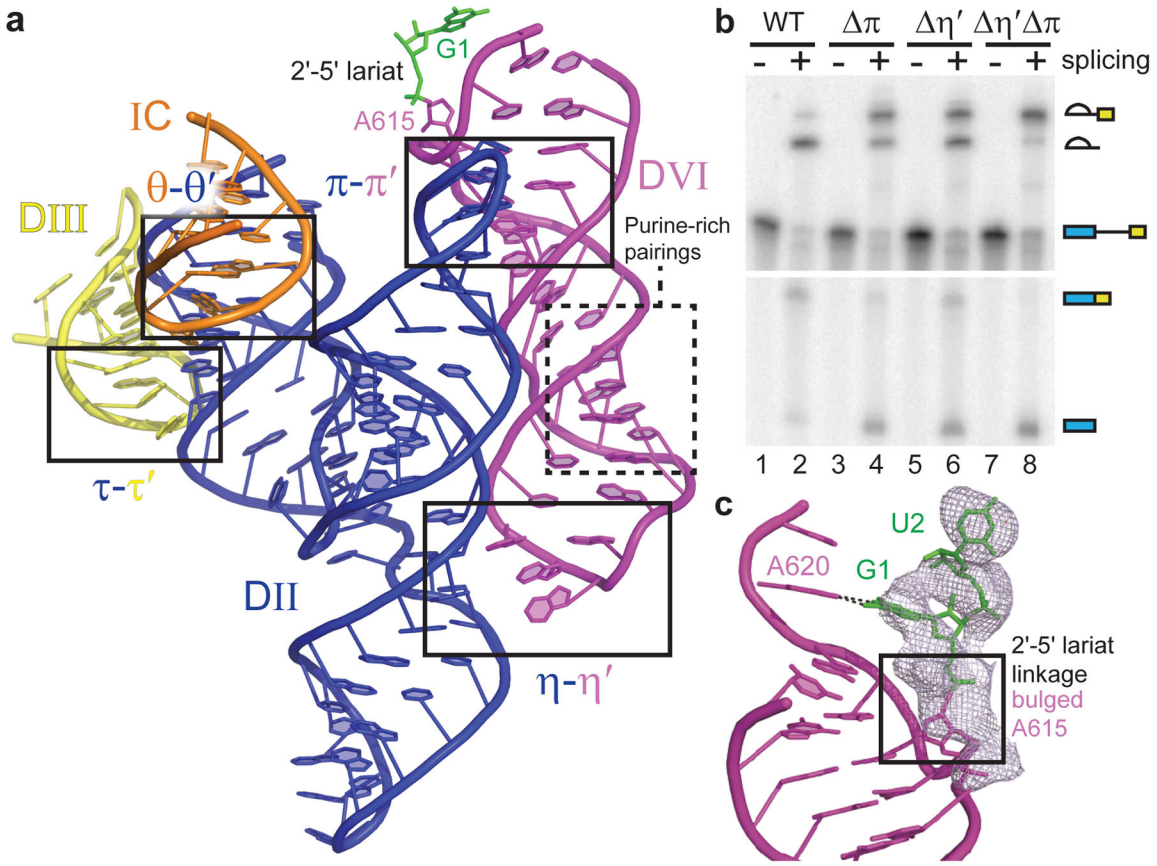

Figure 3.

The position of DVI within the intron structure. **a**, DII forms an inverted Y-shaped structure that engages in four distinct tetraloop-receptor interactions with the IC stem (orange), DIII (yellow), and DVI (purple). DVI interacts with DII via two tandem tetraloop-receptor interactions, η-η' and π-π'. **b**, *In vitro* self-splicing assays of the *P.li.LSUI2* intron. The wild-type (WT) intron efficiently catalyzes both steps of splicing and forms intron lariat and ligated exons. Mutagenesis of either η-η' (Δη')[20] or π-π' (Δπ) inhibits the second step, resulting in the accumulation of lariat-3′ exon and 5′ exon. A combination of both mutations (Δη'Δπ) nearly blocks the second step of splicing with predominantly lariat-3′ exon present. **c**, F_o–F_c density for the 2′-5′ lariat phosphodiester bond contoured at 3σ. The nucleobase of A615 is disordered and not visualized. This map was calculated using a model deleted for A615, G1, and U2 (shown in stick format) to avoid model bias. The 5′ (G1) and 3′ (A620) ends form a non-canonical base pair.

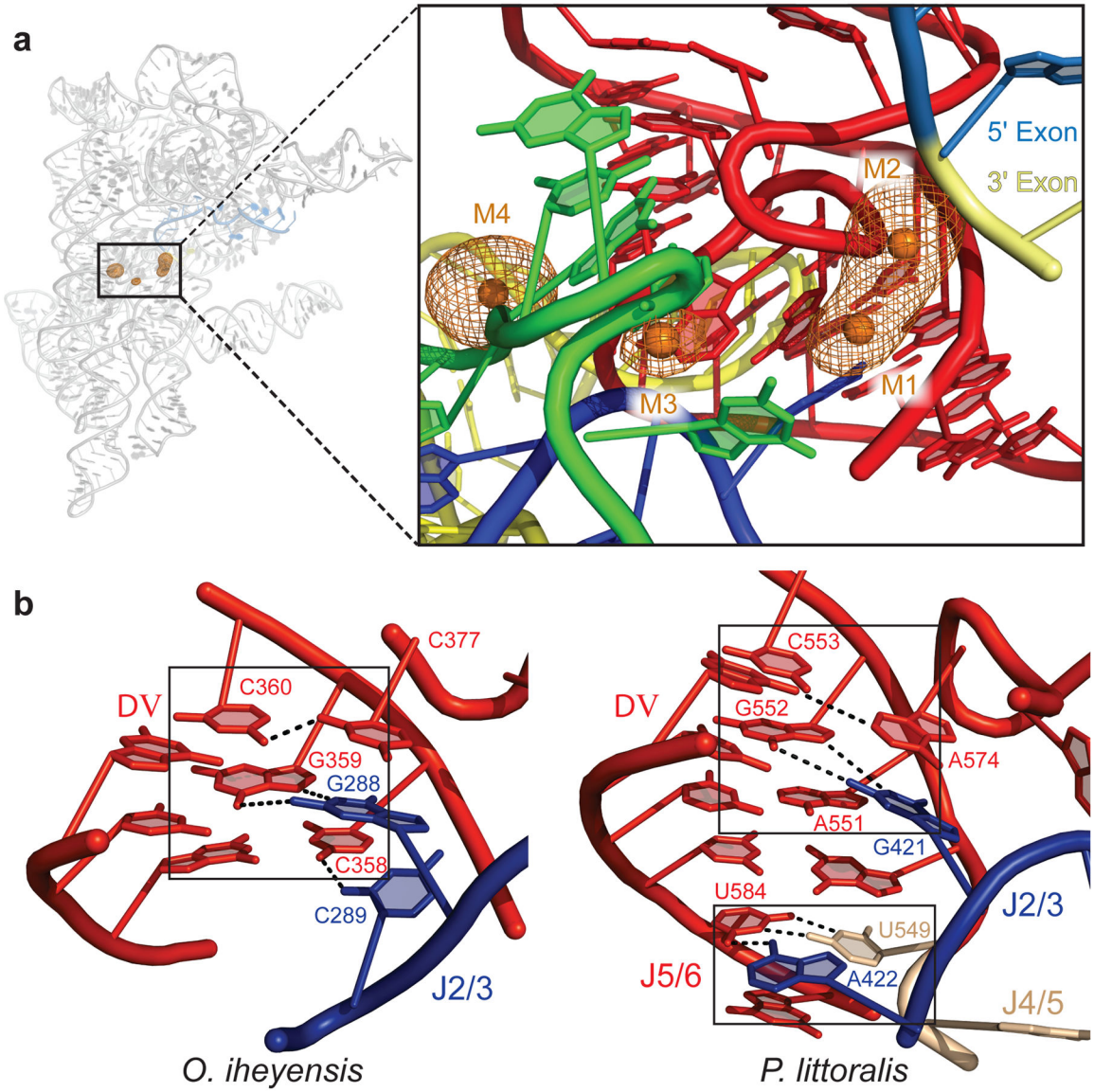

Figure 4.

The core of the of *P.li.LSUI2* intron. **a**, Yb^{3+} anomalous map (orange mesh) contoured at 12σ reveals four large peaks, which correspond to highly-coordinated magnesium ions (orange spheres). **b**, Comparison of the catalytic triplexes found in the *O. iheyensis* and *P.li.LSUI2* introns. *O. iheyensis* contains a continuous triple helix spanning between the DV catalytic triad (CGC) and J2/3. In *P.li.LSUI2*, the J2/3 residue A422 is disengaged from the catalytic triad (AGC) and forms a base triple with J4/5 and J5/6 nucleotides (U549 and U584, respectively).

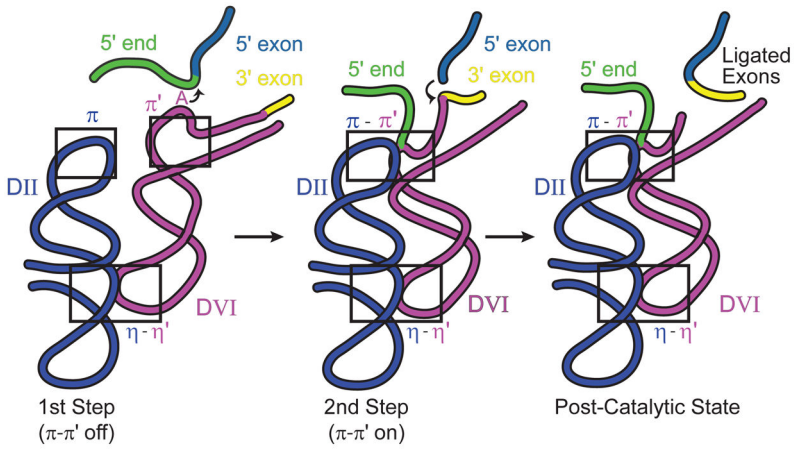

Figure 5.

Model for DVI as the conformational switch for splicing. π-π' mediates the transition between the two steps of catalysis. See text for details.